Liquid Crystals
Publication details, including instructions for authors and subscription information:
http://www.informaworld.com/smpp/title~content=t713926090

Inversion of the phase sequence between the cubic and smectic C phases under pressure

Yoji Maeda[a]; Hiroyuki Mori[b]; Shoichi Kutsumizu[b]
[a] Department of Nanochemistry, Faculty of Engineering, Tokyo Polytechnic University, Kanagawa, Japan [b] Department of Chemistry, Faculty of Engineering, Gifu University, Gifu, Japan

To cite this Article Maeda, Yoji , Mori, Hiroyuki and Kutsumizu, Shoichi(2009) 'Inversion of the phase sequence between the cubic and smectic C phases under pressure', Liquid Crystals, 36: 3, 217 — 223
To link to this Article: DOI: 10.1080/02678290902814692
URL: http://dx.doi.org/10.1080/02678290902814692

Liquid Crystals,
Vol. 36, No. 3, March 2009, 217–223

Taylor & Francis
Taylor & Francis Group

PRELIMINARY COMMUNICATION

Inversion of the phase sequence between the cubic and smectic C phases under pressure

Yoji Maeda[a]*, Hiroyuki Mori[b] and Shoichi Kutsumizu[b]

[a]*Department of Nanochemistry, Faculty of Engineering, Tokyo Polytechnic University, 1583 Iiyama, Atsugi, Kanagawa 243-0297, Japan;* [b]*Department of Chemistry, Faculty of Engineering, Gifu University, 1-1 Yanagido, Gifu 501-1193, Japan*

(Received 12 December 2008; final version received 11 February 2009)

The phase behaviour of a thermotropic cubic mesogen of 1,2-bis(4′-*n*-tetradecyloxybenzoyl)hydrazine BABH-14 was studied under hydrostatic pressure using a polarising optical microscope equipped with a high-pressure optical cell, and the *P–T* phase diagram was constructed. BABH-14 shows the Cr–Cub–I transition sequence under atmospheric and lower pressures, but the Cub phase is replaced completely by the high-pressure SmC, SmC(hp), phase under higher pressures. There is a narrow intermediate-pressure region between the low- and high-pressure regions, in which the Cr–SmC(hp)–Cub–I phase sequence is recognised. The SmC(hp)–Cub transition line has a positive slope with pressure and there are two triple points: one is for the Cr, Cub and SmC(hp) phases and the other is for the I, Cub and SmC(hp) phases. Comparing the phase sequence of BABH-14 with those for BABH-8 and -10, the pressure-induced inversion of the phase sequence between the cubic and SmC phases occurs in the BABH-*n* homologous compounds. Another new phenomenon is the formation of the monotropic cubic phase on cooling in the intermediate- and high-pressure regions, and an intriguing phenomenon of the cubic phase appearing twice, i.e. I–Cub–SmC(hp)– Cub–Cr phase transition, occurs in the intermediate-pressure region.

Keywords: thermotropic cubic mesogen; inversed phase sequence; cubic and smectic C phases; hydrostatic pressure; monotropic cubic phase

1. Introduction

Very much of interest is the thermotropic cubic mesophase of bicontinuous type in which three-dimensional structural periodicity is realised for optical isotropy. 1,2-bis(4′-*n*-alkyloxybenzoyl)hydrazine, abbreviated as BABH-*n* (*n* indicating the number of carbon atoms in the alkoxy group) is known as one of classical thermotropic cubic mesogens. BABH-*n* molecules are composed of a rigid aromatic core at the centre and flexible aliphatic chains at the molecular ends. The chemical structure of BABH-*n* is:

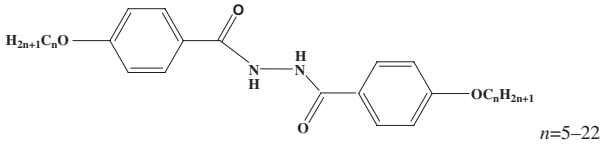

As reported by Schubert and Demus *et al.* (*1*,*2*) BABH-8, -9, and -10 having octyloxy, nonyloxy, and decyloxy groups, respectively, exhibit the cubic (Cub) and smectic C (SmC) phases between the crystal (Cr) and isotropic liquid (I) phases, and they show an unusual phase sequence of Cr–Cub–SmC–I, in contrast to the usual phase sequence of Cr–SmC–Cub–I of many cubic mesogens showing cubic and SmC phases (*3–10*). BABH-8 has the *Ia3d* cubic structure, which consists of two pairs of 3-by-3 interpenetrating networks (*11–13*). Recently, two of the authors extended the previous work and revealed the phase behaviour from $n = 5$ to $n = 22$; the alkoxy chain members other than $n = 8$–10 show the Cr–Cub–I phase sequence under atmospheric pressure (*14–16*). BABH-*n* system exhibits two types of cubic phases, *Ia3d* and *Im3m* types, i.e. BABH-6–BABH-12 and BABH-17–BABH-22 take the *Ia3d* type, and BABH-14 has the *Im3m* type. BABH-13, -15 and -16 have both types.

The authors reported the *P–T* phase diagrams of BABH-8 (*17*) and BABH-10 (*18*) and, although partly incomplete, the phase diagrams of BABH-11 and -12 (*19*) using mainly a high-pressure differential thermal analyser. In BABH-8 and -10, the Cr–Cub and SmC–I transition lines show typically positive slopes (dT/dP) with pressure, while the Cub–SmC transition line exhibits a negative slope. Accordingly, a triple point appears at a relatively low pressure in which the Cr, Cub and SmC phases meet. Their triple points are reported to be about 32 and 11 MPa for BABH-8 and -10, respectively, indicating the upper limit of pressure for the formation of the cubic phase. In the higher pressure region the SmC phase is held as only one mesophase. On the other hand, BABH-11 and -12 show the Cr–Cub–I phase sequence under

*Corresponding author. Email: ymaeda@nano.t-kougei.ac.jp

ISSN 0267-8292 print/ISSN 1366-5855 online

DOI: 10.1080/02678290902814692
http://www.informaworld.com

atmospheric and low pressures below 10–11 and 16–17 MPa, respectively, beyond which the cubic phase is replaced completely by a high-pressure SmC phase. In this case the SmC phase is a high-pressure phase, named here as SmC(hp), because the phase goes back to the cubic phase when pressure is released to atmospheric pressure. Unfortunately, the Cub–SmC(hp) transition lines are not determined yet in the phase diagrams of BABH-11 and -12, but only the maximum pressure for the cubic phase is deduced (*19*).

In this paper, the phase transition behaviour of BABH-14 was studied under hydrostatic pressures using a polarising optical microscope (POM) equipped with a high-pressure optical cell (*20*). BABH-8 also was reinvestigated for comparison.

2. Experimental

BABH-8 and -14 samples used in this study were prepared as described elsewhere (*14–16*). The morphological observation was performed using an Olympus BX51 POM equipped with the high-pressure optical cell system. The high-pressure system uses silicone oil having a low viscosity (10 centi-Stokes, Toshiba Silicone Co., TSF 451-10) as the pressure medium and the system can apply hydrostatic pressure up to 200 MPa. The intensity of transmitted light under crossed polarisers was measured using the Mettler FP-90 photomonitor, in order to determine precisely the transition points. Texture observation and intensity measurement of transmitted light were performed simultaneously on both heating and cooling at a scanning rate of 1–2°C/min under pressures up to 120 MPa. A preliminary X-ray analysis of the mesophases under pressure was performed using a rotating anode X-ray apparatus, Rigaku Rint2500, equipped with a high-pressure sample vessel on the wide-angle goniometer (*21*). A Ni-filtered Cu Kα X-ray beam was directed at the sample under hydrostatic pressure, and wide-angle X-ray diffraction (WAXD) patterns were obtained using an imaging plate (BAS-IP 127×127 mm^2, Fuji Photo Film Co.). The camera length was 100 mm.

BABH-8 and -14 take the reversible phase transitions of Cr-136.4-Cub-156.9-SmC-164.4-I and Cr-129.4-Cub-159.2-I, respectively (transition temperature in °C). The cubic and isotropic liquid phases are usually observed as a completely black field of view under crossed polarisers due to the optical isotropy. However, the use of sapphire as the top and bottom optical windows in the high-pressure optical cell makes these textures appear as a bright field of view because POM light can pass partly through. Thus the discrimination between the cubic and isotropic liquid phases can be made easily under hydrostatic pressure.

3. Results and discussion

Figure 1 shows the POM textures of BABH-8 and -14 observed on cooling from the isotropic liquid at 3.5 and 25 MPa, respectively. The textures (from top to bottom) for BABH-8 at 3.5 MPa show (a) the isotropic liquid at 159°C, (b) the SmC phase at 150°C, (c) the cubic phase at 138°C, and (d) the crystalline phase at 120°C in the left row, respectively. Figure 2 shows the intensity (I) of transmitted light vs. temperature (T) curves of BABH-8 on heating at (a) 3.5 and (b) 30 MPa. The I–T curves show clearly the step-by-step change at each phase transition so that the transition points are determined clearly. The (a) and (b) curves exhibit the representative I–T curves in the low- and high-pressure regions, indicating the Cr–Cub–SmC–I and Cr–SmC–I phase sequences, respectively. The phase sequences are observed reversibly

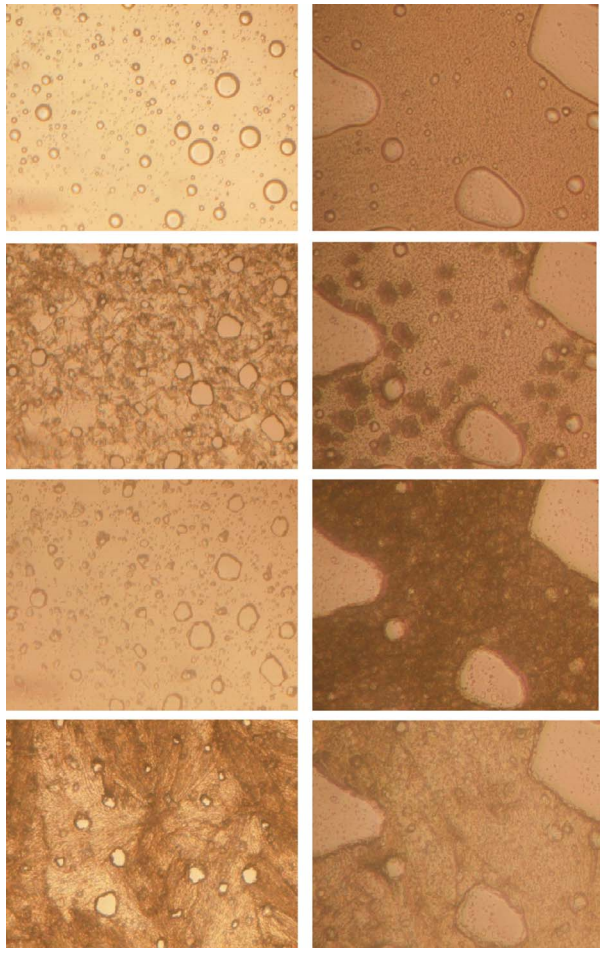

Figure 1. POM textures of BABH-8 (left row) and -14 (right row) observed on cooling at 3.5 and 25 MPa, respectively: (from top to bottom), the isotropic liquid at 159°C, the SmC phase at 150°C, the Cub phase at 138°C, and the Cr phase at 120°C in the left row; the Cub phase at 158°C, the Cub–SmC(hp) transition at 146°C, the SmC(hp) phase at 140°C, and the monotropic Cub phase at 135°C in the right row.

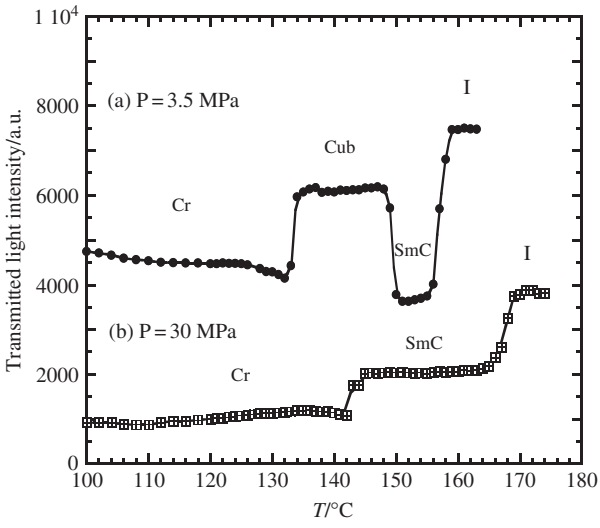

Figure 2. *I–T* curves of BABH-8 at (a) 3.5 MPa and (b) 30 MPa.

under pressures, and the former one is seen under pressures below about 13 MPa.

Applying pressure on the cubic phases of BABH-11 and -12 induces the formation of the high-pressure SmC phase (*19*). The phase behaviour of BABH-14 under pressure is similar to that of BABH-12. Figure 3 shows three *I–T* curves of BABH-14 on heating and cooling at 15.0, 27.5 and 61.5 MPa, respectively. The analysis of the *I–T* curves allows us to divide the phase behaviour into three pressure regions, i.e., a low-pressure region below about 15 MPa, an intermediate-pressure region between 15 and 37 MPa, and a high-pressure region above 37 MPa. The *I–T* curves at 15.0 MPa show the reversible changes in two steps from the crystal to the isotropic liquid via the cubic phase in which the same transition sequence as at atmospheric pressure is observed. The *I–T* curve on heating at 27.5 MPa changes by three steps from the crystal to the isotropic liquid via the SmC(hp) and cubic mesophases. On the succeeding cooling, the intensity decreases first at the I–Cub transition, and it recovers slightly with decreasing temperature in the cubic phase. There is then a large but slow decrease in intensity, depending upon the progress of the Cub–SmC(hp) transition on cooling.

The optical micrographs in the right row of Figure 1 show the POM textures of BABH-14 observed on cooling from the isotropic liquid at 25 MPa. The textures (from top to bottom) exhibit the cubic phase at 158°C, the co-existent state of the cubic and SmC(hp) phases at 146°C, the SmC(hp) phase at 140°C, and an unknown phase at 135°C. The cubic phase appears first as a sand-like texture and then the SmC(hp) phase is formed sporadically as dark lumps in the sand-like texture. They grow up slowly to the dark texture of

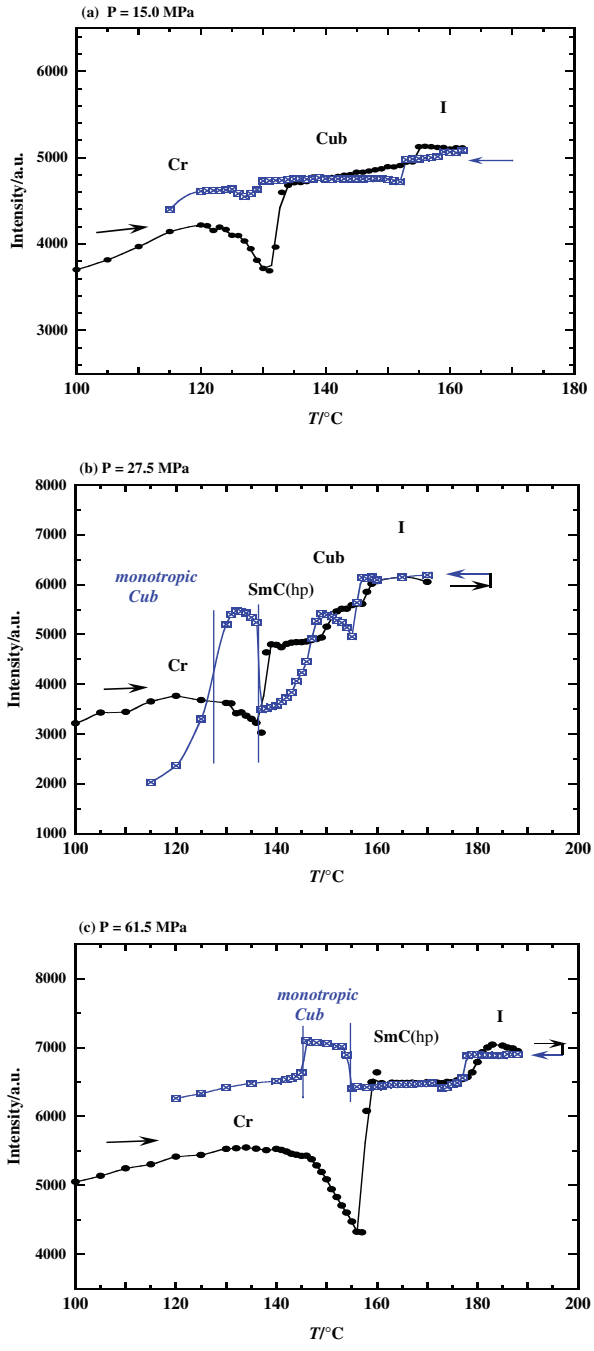

Figure 3. *I–T* curves of BABH-14 at (a) 15 MPa, (b) 27.5 MPa, and (c) 61.5 MPa.

the SmC(hp) phase in the entire field of view on cooling. The dark texture changes suddenly to a bright one for the unknown phase, named here as X phase. The X phase shows no characteristic texture and an abrupt increase of intensity comparable to one of the cubic phases in the *I–T* curve. Such state is held in a temperature region of about 5–10°C. Finally, the bright texture changes rapidly to the solid-like texture at the crystallisation temperature and the intensity decreases with

decreasing temperature. The *I–T* curve on heating at 61.5 MPa changes by two steps from the crystal to the isotropic liquid via the SmC(hp) phase, showing the simple Cr–SmC(hp)–I phase sequence. On the succeeding cooling, the intensity first slips down at the I–SmC(hp) transition. Many bright spheres of the SmC(hp) phase appear in the bright field of view for the isotropic liquid at 176°C, and the spheres grow rapidly and then coalesce to form the continuous textures of the high-pressure SmC phase. The SmC(hp) phase is stable across a relatively wide temperature region. The intensity then increases sharply to the level of the isotropic liquid, indicating the formation of the monotropic X phase at 154°C. Finally, the intensity decreases at the X–Cr transition, and then decreases gradually on further cooling.

There is a boundary region between the low- and high-pressure regions, named here as the intermediate-pressure region, in which both the cubic and SmC(hp) phases appear. In this region the phase sequence of I–Cub–SmC(hp)–*monotropic X*–Cr is recognised on cooling, as seen in the right row of Figure 1. The cubic phase appears first as the high-temperature phase, and then the SmC(hp) and monotropic X phases are observed successively. Since the monotropic X phase shows no characteristic texture and strong transmitted light comparable with that of the cubic and isotropic liquid phases, it could be reasonably suggested that the X phase is another cubic phase, different from the stable cubic phase in the low-pressure region. This suggestion is strongly supported by the preliminary X-ray results, shown later. The monotropic cubic phase is thermodynamically metastable because this phase appears only on cooling, and the stable phase is crystal at these temperatures. This phenomenon occurs in the intermediate- and high-pressure regions. Recently, the SmC(hp) and the successive monotropic cubic phases have also been found in BABH-16 and -18, and will be described elsewhere. At present it is unclear why the monotropic cubic phase appears.

Figure 4 shows the *P–T* phase diagrams of BABH-8 and -14. The phase diagram of BABH-8 reported previously (*17*) is supported here: both the Cub–SmC transition line with a negative slope and the existence of a triple point are confirmed. The triple point is estimated at 24 MPa and 144°C this time by extrapolating the Cub–SmC transition line to a higher pressure. This value is more reliable because the Cub–SmC transition line could be determined more precisely. The phase behaviour for BABH-14 is divided into the low-, intermediate- and high-pressure regions. The intermediate-pressure region is clearly determined by the SmC(hp)–Cub transition line having a positive slope (d*T*/d*P*). Two triple points can be seen; one is for

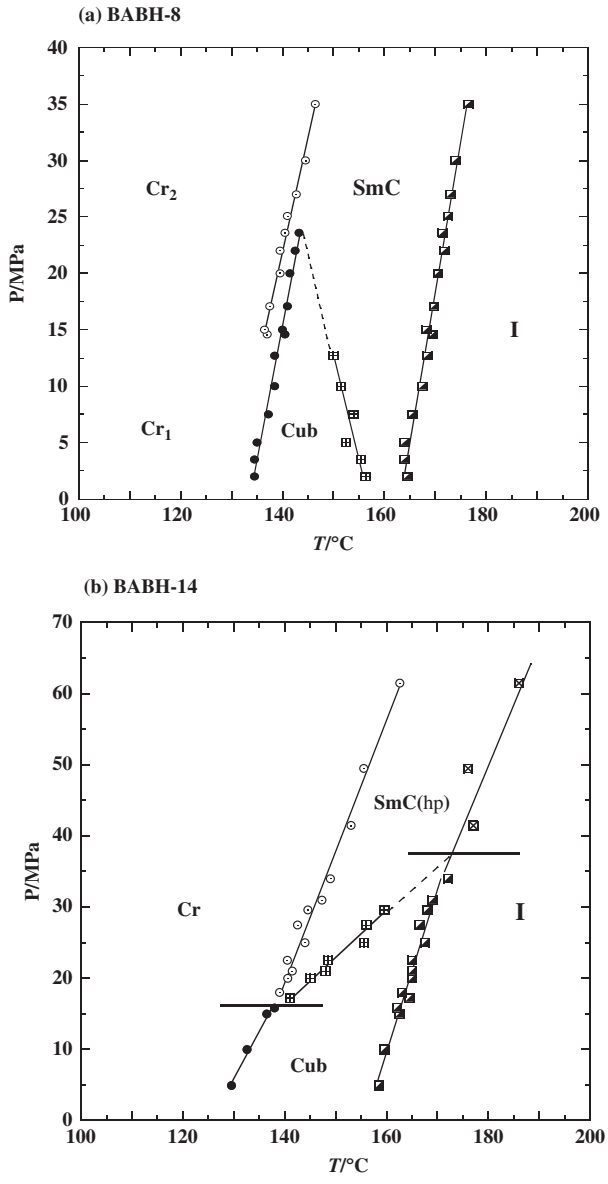

Figure 4. *P–T* phase diagrams of BABH-8 and -14.

the Cr, Cub and SmC(hp) phases, indicating the lower limit of pressure for the formation of the SmC(hp) phase, and the other is for the I, Cub, and SmC(hp) phases, indicating the upper limit of pressure for the cubic phase. The phase sequences, the pressure regions, the slopes of the Cub-SmC transition line, and the triple points for the BABH-8 and -14 samples are listed in Table 1.

It is noteworthy that the slope of the Cub–SmC (or SmC–Cub) transition line changes from negative to positive values with increasing length of the alkoxy chains of the BABH-*n* samples. What should be noted here is that in BABH-14 the high-pressure SmC phase appears at the low-temperature side of

Table 1. Phase behaviour of BABH-8 and -14 under pressure.

	Phase sequence		
Pressure region	BABH-8	BABH-14	
Low-pressure region/MPa	*Cr - Cub - SmC - I* **0.1 ~ 24**	*Cr - Cub - I* **0.1 ~ 15**	
		Cr → *SmC*(hp) - *Cub* – *I* ↖ ↙ *Cub*	
Intermediate-pressure region/MPa	----- *Cr - SmC - I*	**15 ~ 36** *Cr* → *SmC*(hp) – *I* ↖ ↙ *Cub*	
High-pressure region/MPa	**>24**	**>36**	
Slope of Cub-SmC (or vice versa) transition / °C MPa^{-1}	**–0.5**	**+1.5**	
Triple point			
P/**MPa**	**24**	**15**	**36**
T/°C	**144**	**133**	**163**

the stable cubic phase in the intermediate-pressure region. The SmC(hp)–Cub transition line exhibits a positive slope (d*T*/d*P*) with pressure, which is usually observed in 4'-*n*-alkyloxy-3'-nitrobiphenyl-4-carboxylic acids having alkoxy chains containing 16, 20 and 22 carbon atoms, referred to as ANBC-16, -20, and -22, respectively (*22*). This means that the unusual phase sequence of Cr–Cub–SmC–I in BABH-8 and -10 changes inversely to the usual phase sequence of Cr–SmC(hp)–Cub–I for BABH-14 in the intermediate-pressure region. The inversed phase sequence is explained well by Saito and Sorai's 'alkyl-chain as entropy-reservoir' mechanism (*23–26*). Based on the thermodynamic analysis of the entropy of transition between the cubic and SmC phases, they addressed the contribution to the entropy of transition from the aromatic core at the centre and from the alkoxy chains showing opposite signs. This competition accounts for the inversion of the phase sequence in ANBC (SmC→Cub) and BABH (Cub→SmC). The results in this study exhibit that the inversion between the Cub and SmC phases occurs only by applying appropriate pressures on the homologous series of BABH-*n* samples with different lengths of alkoxy chains. To the best of our knowledge, this is the first example of pressure-induced inversion of the phase sequence between the cubic and SmC phases in liquid crystalline compounds.

The X-ray patterns of the *Im3m*-cubic phase in the low-pressure region, the high-pressure SmC phase and monotropic cubic phase in the high-pressure region were obtained by the WAXD measurements of BABH-14 under hydrostatic pressure. Figure 5 shows the *P–T* phase diagram constructed on cooling and the X-ray patterns which are magnified in the low-angle region of (a) the *Im3m*-Cub phase at 140°C and 5 MPa, (b) the cubic phase at 154°C and 26 MPa, (c) the SmC(hp) phase at 165°C and 50 MPa, and (d) the monotropic cubic phase at 150°C and 50 MPa. The high-pressure SmC phase at 50 MPa shows a Debye-Sherrer ring at about 2θ = 2.80° (d = 3.20 nm), indicating the completely random orientation of the lamellar structure. The reflection shows the {001} reflection which exhibits the layer thickness of the SmC(hp) phase. On the other hand, two spot-like patterns for the cubic phases at (a) 5 and (b) 26 MPa are clearly different to each other. Since BABH-14 has the *Im3m*-cubic structure at atmospheric pressure (*15*,*16*), the X-ray pattern at 5 MPa belongs to the *Im3m* structure. The X-ray pattern of the cubic phase at 154°C and 26 MPa is very similar to those for BABH-8 and -12 under atmospheric pressure, which is reduced to the {211} and {220} reflections of the cubic phase with *Ia3d* space group (*13*). The pattern of the monotropic cubic phase at 50 MPa is relatively similar to the *Ia3d*-Cub phase. The preliminary X-ray results strongly suggest that the monotropic cubic phase under high pressure has the *Ia3d* structure. Precise X-ray characterisation for the monotropic cubic structure and other mesophases should be performed for the accurate identification by low-angle X-ray diffraction.

Another interesting finding is that the monotropic cubic phase appears accompanied with the formation of the high-pressure SmC phase for BABH-14 in the

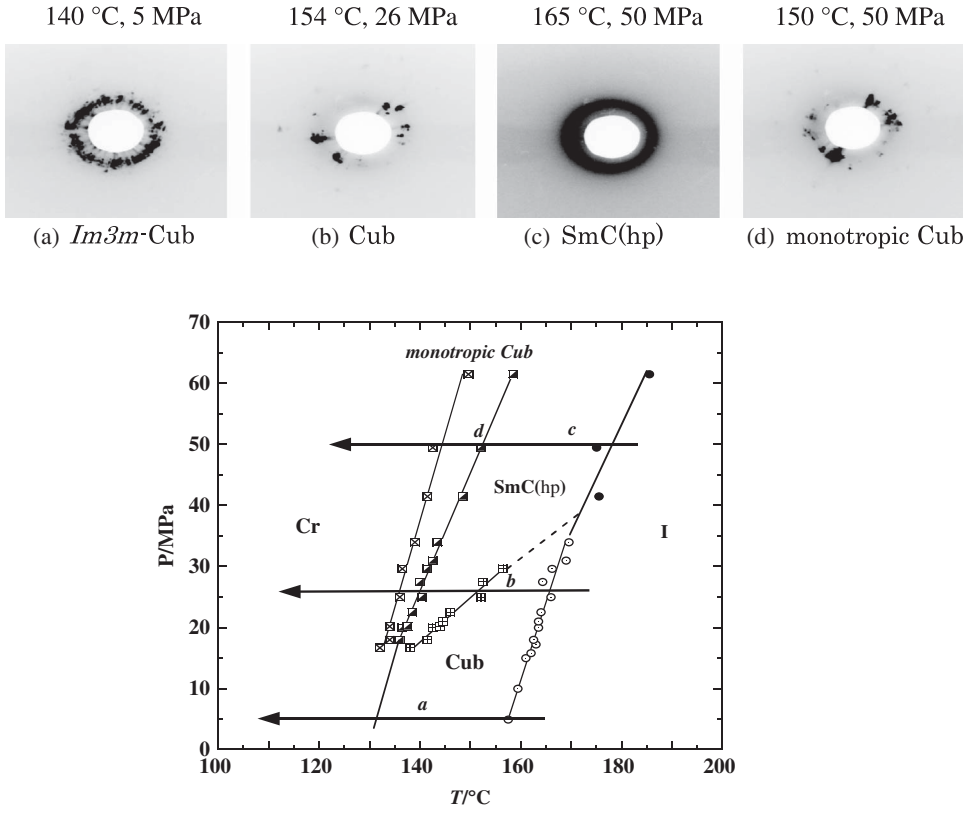

Figure 5. *P–T* phase diagram constructed on cooling and the attached X-ray patterns of BABH-14: (a) *Im3m*-Cub phase at 140°C and 5 MPa, (b) cubic phase at 154°C and 26 MPa, (c) the SmC(hp) phase at 165°C and 50 MPa, and (d) the monotropic Cub phase at 150°C and 50 MPa.

intermediate- and high-pressure regions. It is particularly noted here that the cubic phase for BABH-14 appears twice on cooling in the intermediate-pressure region. This phenomenon may be a kind of re-entrant phenomenon (*27,28*). However, there is another plausible interpretation for this phenomenon because BABH-*n* has two cubic structures with the *Ia3d* and *Im3m* space groups, depending upon the carbon number *n* of alkoxy chains of BABH-*n*: BABH-8, -10, -11, -12 and -18 take the *Ia3d* structure, but BABH-14 has the *Im3m* structure. BABH-13, -15 and -16 exhibit the two cubic structures under atmospheric pressure (*14–16*). Therefore, the two kinds of cubic structures for BABH-14 might appear on cooling in the intermediate-pressure region. This problem is a very intriguing question, and should be clarified experimentally by low-angle X-ray analysis under hydrostatic pressure.

Acknowledgements

S.K. is grateful for financial support from the Ministry of Education, Culture, Sports, Science, and Technology, Japan [Grant-in-Aid for Scientific Research on Priority Area "Super-Hierarchiral Structures" (No. 446/19022012)] and from Japan Society for the Promotion of Science [Grant-in Aid for Scientific Research (C) 18550121].

References

(1) Schubert, H.; Hauschild, J.; Demus, D.; Hoffmann, S. *Z. Chem.* **1978**, *18*, 256.
(2) Demus, D.; Gloza, A.; Hartung, H.; Hauser, A.; Rapthel, I.; Wiegeleben, A. *Cryst. Res. Technol.* **1981**, *16*, 1445–1451.
(3) Gray, G.W.; Jones, B.; Marson, F. *J. Chem. Soc.* **1957**, 393–401.
(4) Demus, D.; Kunicke, G.; Neelsen, J.; Sackmann, H. *Z. Naturforsch*. **1968**, *23*, 84–90.
(5) Gray, G.W.; Goodby, J.W., Eds.; *Smectic Liquid Crystals Textures and Structures*; Leonard Hill: Glasgow and London. 1984; pp. 68–81, including earlier references on thermotropic cubic mesogens.
(6) Diele, S.; Göring, P. In *Handbook of Liquid Crystals*, Demus, D.; Goodby, J.; Gray, G.W.; Spiess, H.-W.; Vill, V., Eds.; Wiley-VCH: Weinheim, 1998; Vol. 2B, Chap. XIII. pp. 887–900.
(7) Bruce, D.W.; Dunmer, D.A.; Hudson, S.A.; Lalinde, E.; Maitlis, P.M.; McDonald, M.P.; Orr, R.; Styling, P. *Mol. Cryst. Liq. Cryst.* **1991**, *206*, 79–92.
(8) Donnio, B.; Heinrich, B.; Gulik-Krywicki, T.; Delacroix, H.; Guillon, D.; Bruce, D.W. *Chem. Mater.* **1997**, *9*, 2951–2965.

(9) Rowe, K.E.; Bruce, D.W. *J. Mat. Chem.* **1998**, *8*, 331–341.
(10) Donnio, B.; Bruce, D.W. *J. Mat. Chem.* **1998**, *8*, 1993–1997.
(11) Luzzati, V.; Spegt, P.A. *Nature* **1967**, *215*, 701–704.
(12) Schoen, A.H. *NASA Tech. Note* No. D-5541, 1970, pp. 1–92.
(13) Göring, P.; Diele, S.; Fischer, S.; Wiegeleben, A.; Pelzl, G.; Stegemeyer, H.; Thyen, W. *Liq. Cryst.* **1998**, *25*, 467–474.
(14) Mori, H.; Kutsumizu, S.; Ito, T.; Fukatami, M.; Saito, K.; Sakajiri, K.; Moriya, K. *Chem. Lett.* **2006**, *35*, 362–363.
(15) Kutsumizu, S.; Mori, H.; Fukatami, M.; Saito, K. *J. Appl. Crystallogr*. **2007**, *40*, s279–s282.
(16) Kutsumizu, S.; Mori, H.; Fukatami, M.; Naito, S.; Sakajiri, K.; Saito, K. *Chem. Mater.* **2008**, *20*, 3675–3687.
(17) Maeda, Y.; Saito, K.; Sorai, M. *Liq. Cryst.* **2003**, *30*, 1139–1149.
(18) Maeda, Y.; Ito, T.; Kutsumizu, S. *Liq. Cryst*. **2004**, *31*, 623–632.
(19) Maeda, Y.; Ito, T.; Kutsumizu, S. *Liq. Cryst*. **2004**, *31*, 807–820.
(20) Maeda, Y.; Koizumi, M. *Rev. Sci. Instrum.* **1996**, *67*, 2030–2031; Maeda, Y.; Koizumi, M. *Rev. High Pressure Sci. Technol.* **1998**, *7,* 1532–1534.
(21) Maeda, Y.; Kanetsuna, H. *Bull. Res. Inst. Polym. Tex.* **1985**, *149*, 119–125; Maeda, Y. *Thermochimica Acta*, **1990,** *163*, 211–218.
(22) Maeda, Y.; Morita, K.; Kutsumizu, S. *Liq. Cryst.* **2003**, *30*, 157–164.
(23) Saito, K.; Sato, A.; Sorai, M. *Liq. Cryst.* **1998**, *25*, 525–530.
(24) Sato, A.; Yamamura, Y.; Saito, K.; Sorai, M. *Liq. Cryst.* **1999**, *26*, 1185–1195.
(25) Saito, K.; Sorai, M. *Chem. Phys. Lett*. **2002**, *366*, 56–61.
(26) Sorai, M.; Saito, K. *Chem. Rec*. **2003**, *3*, 29–39.
(27) Cladis, P.E. In *Handbook of Liquid Crystals*, ed. by Demus, D.; Goodby, J.; Gray, G.W.; Spiess, H.-W.; Vill, V., Eds.; Wiley-VCH: Weinheim, 1998; Vol.1, Chap. VI-4. pp. 391–403.
(28) Cladis, P.E.; Bogardus, R.K.; Daniels, W.B.; Taylor, G.N. *Phys. Rev. Lett.* **1977**, *39*, 720–723; Cladis, P.E.; Bogardus, R.K.; Aadsen, D. *Phys. Rev. A* **1978**, *18*, 2292–2306.